RSC Advances

ROYAL SOCIETY
OF CHEMISTRY

www.rsc.org/advances

RSC Advances

ARTICLE

Enhancement of Photo-catalytic Degradation of Formaldehyde through Loading Anatase TiO$_2$ and Silver Nanoparticle Films on Wood Substrates

Likun Gao[1], Wentao Gan[1], Shaoliang Xiao[1], Xianxu Zhan[2*], Jian Li[1*]

Since formaldehyde is considered as a potential risk for human health, its emission must be eliminated in an effective way. In this study, anatase TiO$_2$ particles with silver nanoparticles were doped on wood substrates through a two-step method and used as a photo–catalyst for formaldehyde degradation. The effect of Ag dopant on the formaldehyde degradation of the TiO$_2$–treated wood was investigated. The results showed that the formaldehyde response of TiO$_2$ film was drastically improved by doping with Ag nanoparticles under the visible–light irradiation. In this heterostructured system, because the Fermi level of Ag was lower than the conduction band of TiO$_2$, Ag nanoparticles can act as electron scavenging centers for causing electron and hole pair separation, leading to an enhanced photo–catalytic activity of TiO$_2$.

Keywords: silver nanoparticles, anatase TiO$_2$, formaldehyde degradation, visible light, wood

Introduction

As a significant volatile organic compounds (VOCs), Formaldehyde (HCHO) is considered as one of the most important pollutants in indoor environment.[1, 2] Wood-based products are under the category of natural materials due to their friendly properties of health, aesthetic and environmental aspects. However, because the urea-formaldehyde adhesives in wooden panels could produce HCHO gas during the application, the fear of the formaldehyde emission limits the use–value of wooden panels.[3] Although the elimination of formaldehyde is very difficult, the photo–decomposition was proved to be a promising method to remove gaseous pollutants.[4, 5] Furthermore, due to the increasing concern on HCHO in the indoor environment, the abatement of HCHO is of significant practical interest at low temperature, especially at room temperature. Very recently, many studies on the reduction of HCHO by adsorbents or catalysts were reported.[6-8] However, the reclamation of the catalysts, such as powder and particles, plays a critical role in the practical applications, which would influence the development of environmental technology for decontamination, purification, and deodorization of the

[a.]Material Science and Engineering College, Northeast Forestry University, Harbin 150040, P.R. China
[b.]Dehua TB New Decoration Material Co., Ltd, Huzhou, 313200, P.R. China
*Corresponding author. Tel: +86-451-82192399; fax: +86-451-82192399
E-mail addresses: gaolknefu@163.com(Likun Gao), and nefulijian@163.com (Jian Li).

atmospheres. Based on above consideration, the wood−based products composited with a film of catalysts were proposed. The planned treatment would not only produce a catalyst for decomposition of the toxic organic pollutants, but also fundamentally modified the wood substrates.

Since Fujishima reported UV irradiation induced redox chemistry on TiO_2, photo−catalysis has attracted the most interest as a green and sustainable solution for energy and environmental issues.[9, 10] As an *n*−type semiconductor oxide, TiO_2 is widely used as photo−catalyst in the applications such as self-cleaning, self-degradation, etc., because it is relatively inexpensive and can degrade toxic contaminants without requiring other reagents.[11, 12] Up to now, an increasing attention has been paid to improve its physical and chemical properties, which would further facilitate the profound understanding of the dependence of material properties. Driven by this requirement, great amount of innovative approaches have been conducted to develop novel semiconductor−based composites with desired properties and functions for special applications. In order to endow the TiO_2−based materials with extraordinary properties and superb photocatalytic performance in practical applications, the method of metal doped TiO_2, such as Ag/TiO_2 composites, has become one of the most attractive candidate solution.[7, 13, 14] Among numerous metals, such as Ru^{15}, $Au^{16, 17}$, $Bi^{18, 19}$, $Pt^{20, 21}$, etc., Ag is particularly suitable for industrial applications because of its low cost and nontoxic properties compared to other noble metals.[14,22] In addition, Ag has a good light absorption capability, extending the response of TiO_2 to visible light.[23, 24]

In this study, because formaldehyde was considered as a main indoor pollutant, it was chosen as the aim pollutant, and wood was selected as substrates coated by TiO_2 particles and silver nanoparticles. The photo−catalytic degradation characters of HCHO by the TiO_2−treated wood and the Ag−doped TiO_2/wood under visible−light irradiation was characterized by the scanning electron microscopy (SEM), transmission electron microscopy (TEM), X−ray diffraction (XRD), X−ray photoelectron spectroscopy (XPS), and UV−vis diffuse reflectance spectroscopy (UV−vis DRS). The analogue experiments of formaldehyde degradation were performed and the mechanism was explored simultaneously.

Methods

Materials

All chemicals supplied by Shanghai Boyle Chemical Company Limited were of analytical reagent-grade quality and used without further purification. The Formaldehyde used in our experiment was an analytical reagent. Deionized water was used throughout the study. The wood blocks of 20 mm (R)×20 mm (T)×30 mm (L) were obtained from the sapwood sections of poplar (*Populus ussuriensis* Kom), which is one of the most common tree species in the northeast of China. After ultrasonically rinsing in deionized water for 30 min, the wood specimens were oven−dried (24 h, 103 °C) to a constant weight, and the weights were determined.

Preparation of anatase TiO_2 film on the wood surface

The Ammonium fluorotitanate (0.4 M) and boric acid (1.2 M) were dissolved in the distilled water in a 500 mL glass container at a room temperature with vigorous magnetic stirring. A solution of 0.3 M hydrochloric acid was added until the pH value reached approximately 3. Then, the 75 mL adjusted solution was transferred into a 100 mL Teflon container. Wood specimens were subsequently placed into the solution, separately. The autoclave was sealed and maintained at 90 °C for 5 h, and then naturally cooled to room temperature. Finally, the treated samples were removed from the solution, ultrasonically rinsed with deionized water for 30 min, and dried at 45 °C for more than 24 h in a vacuum chamber. For the comparative purpose, un-treated wood samples were also examined. As a result, TiO_2 surfaces on the treated wood contained OH groups, which improved the surface hydrophilicity through the TiO_2 hydroxylation.

Loading of the TiO_2−treated wood surface with Ag nanoparticles

Aqua ammonia (28 wt.%) was added dropwise into a 0.5 M $AgNO_3$ aqueous solution with stirring until a transparent colourless $[Ag(NH_3)]^+$ solution was formed. The TiO_2−treated wood samples were soaked to the above solution for 1 h, then transferred to a 0.1 M glucose stock solution. After 5 min, the residual $[Ag(NH_3)]^+$ solution was also poured into the glucose solution. The reaction was continued for 15 min. Finally, the prepared samples were removed from the solution, ultrasonically rinsed with deionized water for 30 min, and dried at 45 °C for more than 24 h in a vacuum chamber. The detailed procedure for the synthesis of the Ag-doped TiO_2/wood heterostructures is illustrated in Scheme 1. In this work, the TiO_2 particles with abundant hydrophilic groups (OH) on the wood surface was dipped into the silver ammonia complex solution, the complexes of $[Ag(NH_3)]^+$ were easily and abundantly absorbed on the TiO_2 particles. And then the silver ammonia complex loaded TiO_2−treated wood was transferred into the solution of glucose and $[Ag(NH_3)]^+$ was in situ reduced into silver seeds on the TiO_2 particles. With the addition of $[Ag(NH_3)]^+$ and glucose, more and more silver ions were absorbed onto the TiO_2−treated wood surface and reduced into silver. The silver seeds grew larger into silver nanoparticles (Ag NPs) and attached to each other forming a compact film on the TiO_2−treated wood.[25]
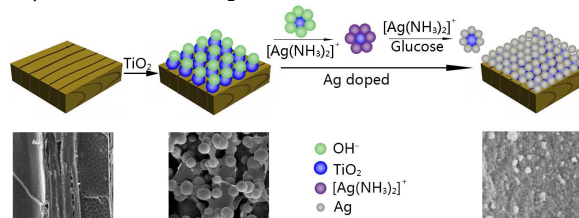
Scheme 1. Schematic representation of the formation of the Ag−doped TiO_2/wood.

Characterization

The morphology of the wood surfaces was observed through the field emission scanning electron microscopy (SEM, Quanta 200, FEI, Holland) operating at 12.5 kV in combination with EDS (Genesis, EDAX, Holland). The transmission electron microscopy (TEM) experiment was performed on a Tecnai G20 electron microscope (FEI, USA) with an acceleration voltage of 200 kV. Carbon−coated copper grids were used as the sample holders. The X−ray diffraction (XRD, Bruker D8 Advance,

Germany) was employed to analyze the crystal structures of all samples applying graphite monochromatic with Cu Kα radiation (λ = 1.5418 Å) in the 2θ range from 5° to 80°and a position−sensitive detector using a step size of 0.02° and a scan rate of 4° min⁻¹. Further evidence for the composition of the product was inferred from the X−ray photoelectron spectroscopy (XPS, Thermo ESCALAB 250XI, USA), using an ESCALab MKII X−ray photoelectron spectrometer with Mg−Kα X−rays as the excitation source. Optical properties of the materials were characterized by the UV−vis diffuse reflectance spectroscopy (UV−vis DRS, Beijing Purkinje TU−190, China) equipped with an integrating sphere attachment, which $BaSO_4$ was the reference.

Photo-catalytic degradation of HCHO

A schematic diagram of the experimental system for photo−oxidation is shown in Scheme 2. The experiments were performed in an obturator with the size of 500 mm (L)×300 mm (W)×300 mm (H). A flat−type LED−light (wavelength is in the range of 400−760 nm, light intensity is approximately 3.6 mW/cm²) installed in the open central region was used to simulate visible light. Initially, there was no HCHO in the obturator, which was detected by a formaldemeter. Then, the desired amount of HCHO was injected into the obturator. The gaseous formaldehyde was allowed to reach adsorption and desorption equilibrium for 30 min. After equilibrium, the initial concentration of formaldehyde in the obturator was controlled in the region of approximately 1.5−2.5 mg/m³. Then, the LED light was turned on to irradiate the sample. Each set of degradation experiment under LED irradiation lasted for 10 h. HCHO concentration in the obturator was determined by the formaldemeter.
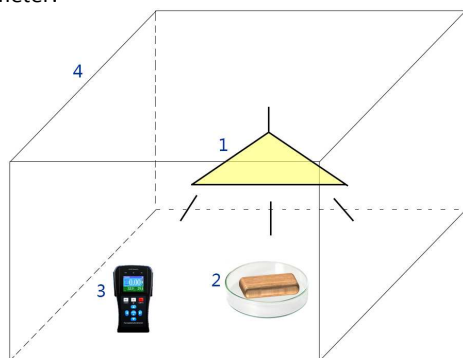
Scheme 2. Schematic diagram of experimental set-up (1. a flat−type LED−light; 2. the treated wood sample; 3. formaldemeter; 4. obturator (500 mm (L)×300 mm (W)×300 mm (H)).

Results and discussion

The SEM images of the un-treated and treated wood samples are presented in Fig. 1. Fig. 1a shows the micrographs of un-treated poplar wood surface, which clearly reveals that the poplar wood is a type of heterogeneous and porous material. Fig. 1b shows that the TiO_2 particles deposit on the wood cell walls and fill into the pits of the wood surface. The TiO_2 particles with the average diameter of approximately 1.5 µm are adhered onto wood surface through the chemical bonds between hydroxyl groups of wood surface and TiO_2

particles. As a comparison of the morphology of pristine TiO_2/wood with that of the Ag nanoparticles doped one, it was observed that a compact layer composed by Ag nanoparticles deposited on its surface (Fig. 1c). The magnified image (Fig. 1d) of the Ag−doped TiO_2/wood demonstrates that the film is approximately 1.8 µm thick and the sphere particles stacked over the wood surface is approximately 130 nm in diameter. The surface chemical elemental compositions of the treated wood are determined via the energy−dispersive X−ray spectroscopy (EDS), and the results are presented in Fig. 1e and Fig. f. The evidence of only fluorine, titanium, gold, and carbon elements could be detected in Fig. 1e, while the additional presence of silver element exists in Fig. 1f. The gold element is originated from the coating layer used for SEM observation, the fluorine element may be originated from the precursor ammonium fluorotitanate, and carbon element was from the wood substrate. Since no other elements were detected, the composition of the microspheres on the TiO_2−treated wood sample was confirmed to be TiO_2 as well as revealing the loading of metallic Ag on the Ag−doped TiO_2/wood sample.
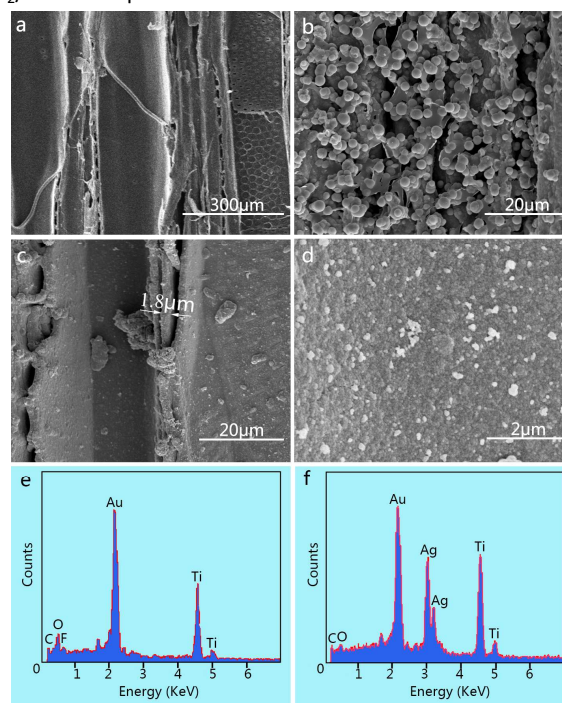

Fig. 1. SEM images of the surfaces of (a) the pristine wood, (b) the TiO_2−treated wood, (c, d) the Ag−doped TiO_2/wood at different magnifications, and (e, f) EDS spectrums of the TiO_2−treated wood and the Ag−doped TiO_2/wood, respectively.

Fig. 2 shows the representative TEM image, the selected electron diffraction (SAED) pattern and high-resolution transmission electron microscopy (HRTEM) image of the Ag−doped TiO_2/wood. As shown in Fig. 2a, the TEM image shows that a large quantity of Ag nanoparticles are attached onto the surface of the TiO_2−treated wood matrix, and the size distribution of Ag nanoparticles is wide. The corresponding selected area electron diffraction (SAED) pattern of the

Ag−doped TiO$_2$/wood is shown in Fig. 2b. The SAED pattern of TiO$_2$ microparticles in anatase phase and Ag nanoparticles in cubic phase shows that the diffraction patterns and rings are co−existent, and the different crystal planes are identified as (101), (200) and (211) diffraction planes of anatase TiO$_2$ as well as (111), (200), (220) and (311) diffraction planes of cubic Ag, respectively.[26] To further investigate the distribution of Ag and TiO$_2$ particles, the HRTEM image is displayed in Fig. 2c. The clear lattice fringe of d−0.35 nm matches that of the (101) plane of anatase phase of TiO$_2$, while the fringe of d−0.24 nm corresponds to the (111) plane of cubic phase of Ag.[7] No other impurities such as silver oxides are detected.
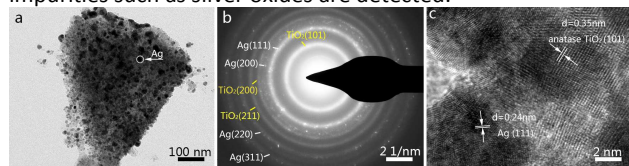

Fig. 2. (a) TEM image, (b) the selected electron diffraction (SAED) patterns, and (c) HRTEM image of the Ag−doped TiO$_2$/wood.

Fig. 3 shows the XRD patterns of the pristine wood, the TiO$_2$−treated wood and the Ag−doped TiO$_2$/wood. Apparently, the diffraction peaks at 14.8° and 22.5° belonging to the (101) and (002) crystal planes of cellulose in the wood are observed in both the spectrum of the pristine wood and the treated wood samples.[27] It can be found that the diffraction peaks are well indexed to the standard diffraction pattern of anatase phase TiO$_2$ (JCPDS file No.21−1272) and the face−centered cubic (fcc) phase of Ag (JCPDS file No.04−0783), indicating that the present synthesis strategy successfully achieves Ag/TiO$_2$ hierarchical heterostructures with high crystallinity on wood substrate. The curve in Fig. 3b shows that the diffraction peaks of pure anatase TiO$_2$ particles center at 2θ = 25.2°, 38.0°, 47.8°, 54.2°, 62.5°, 68.8°, and 74.9°, which agree with (101), (004), (200), (211), (204), (116) and (215) crystal planes of anatase TiO$_2$, respectively.[14] After doped with Ag nanoparticles (Fig. 3c), all of the new diffraction peaks at 38.1°, 44.2°, 64.4°, and 77.4°, except the diffraction peaks of TiO$_2$, can be perfectly indexed to (111), (200), (220) and (311) reflections of the face−centered cubic (fcc) phase of Ag,[7] which is in agreement with SAED pattern results in Fig. 2b.
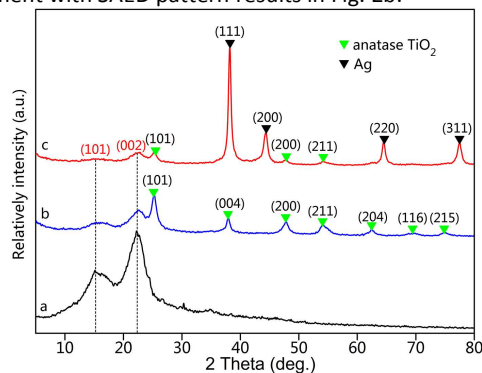

Fig. 3. XRD patterns of (a) the pristine wood, (b) the TiO$_2$−treated wood and (c) the Ag−doped TiO$_2$/wood.

Fig. 4 ascertains more detailed information concerning the elemental and chemical state of the resulting samples. The fully scanned spectra (Fig. 4a) shows that the Ti, O, and C elements exist on the surface of the pure TiO$_2$−treated wood sample, while Ti, O, Ag, and C elements exist on the surface of the Ag−doped TiO$_2$/wood sample. The C element can be ascribed to the wood substrate or the adventitious carbon−based contaminant..
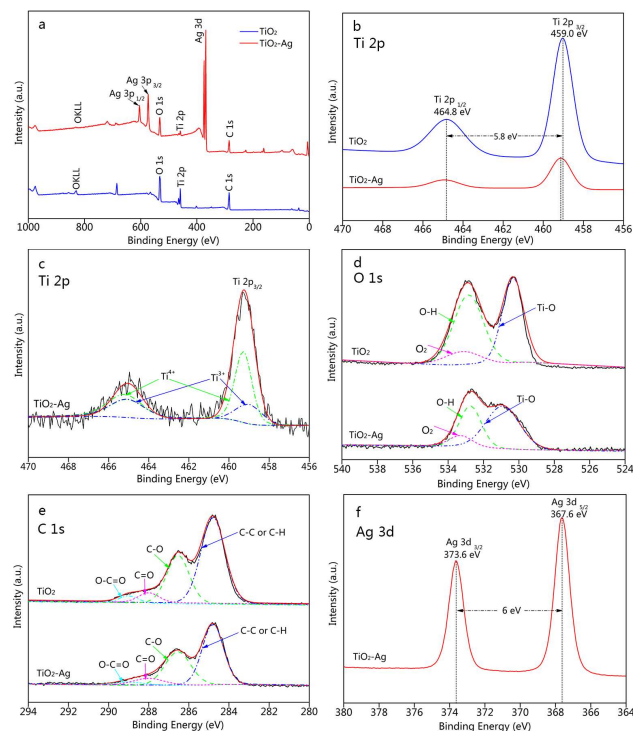

Fig. 4. (a) Survey scan and (b) Ti 2p XPS spectra of TiO$_2$−treated wood and the Ag−doped TiO$_2$/wood, (c) peaking−fitting results of Ti 2p XPS spectra of the Ag−doped TiO$_2$/wood, (d) O 1s and (e) C 1s XPS spectra of TiO$_2$−treated wood and the Ag−doped TiO$_2$/wood, (f) Ag 3d XPS spectra of the Ag−doped TiO$_2$/wood.

From Fig. 4b, the Ti 2p XPS spectra of the TiO$_2$−treated wood with two peaks at binding energies of 459.0 eV and 464.8 eV, corresponding to the Ti 2p$_{3/2}$ and Ti 2p$_{1/2}$ peaks, respectively. The gap of 5.8 eV between the two peaks indicates the existence of the Ti^{4+} oxidation state.[28] However, the peak position for Ti 2p in the Ag−doped TiO$_2$/wood sample shifts to a higher binding energy band than that in the pure TiO$_2$−treated wood sample. This confirms a lower electron density of the Ti atoms after doped with Ag nanoparticles, and there is a strong interaction between metallic Ag and TiO$_2$ in the Ag−doped TiO$_2$/wood. In addition, the Ti 2p$_{3/2}$ XPS peak of the Ag−doped TiO$_2$/wood sample can be fitted into two components, one located at 459.3 eV, attributed to a Ti^{4+} species, and the other located at 458.9 eV, assigned to a Ti^{3+} species (in Fig. 4c), further indicating the strong interaction formed between Ag and TiO$_2$ species. Certainly, the presence of Ti^{3+} oxide with narrow band gap and energy level located between the valence and the conduction band of TiO$_2$ may be

RSC Advances

advantageous to the higher photocatalytic activity of the Ag−doped TiO$_2$/wood heterostructures driven by visible light. Moreover, the defect sites of TiO$_2$ surface induced by light, that is, Ti^{3+} species, are necessary for adsorption and photo−activation of oxygen, which are necessary for the photo−oxidation of pollutants.

The high resolution XPS spectra of O 1s in the TiO$_2$−treated wood and the Ag−doped TiO$_2$/wood are provided in Fig. 4d. The wide and asymmetric O 1s spectra suggests that there would be more than one component. Using the XPS Peak fitting program, version 4.1, the spectra can be further fitted into three peaks including crystal lattice oxygen attributed to the peak of O$_{Ti−O}$ at 530.3 eV, surface hydroxyl groups assigned to the peak of O$_{O−H}$ at 532.8 eV, and adsorbed O$_2$ in molecular water or C−O bonds (at 533.2 eV).[29]

Fig. 4e represents the C 1s XPS spectra of the TiO$_2$−treated wood and the Ag−doped TiO$_2$/wood as well as their fitting results. The spectrum is de-convoluted into four separated Gaussian distributions. The peak around 294.8 eV is assigned to C−C or C−H bonds, and the peak observed at 286.5 eV corresponds to C−O bonds. The other two peaks around 288.0 eV and 289.0 eV are attributed to C=O and O−C=O bonds, respectively, which may be typical for adsorbed carbon on the samples.[30]

As shown in Fig. 4f, the Ag 3d XPS spectra with two peaks at binding energies of 367.6 eV and 373.6 eV, corresponding to the Ag 3d$_{5/2}$ and Ag 3d$_{3/2}$ peaks, respectively. The gap of 6.0 eV between the two peaks is also indicative of metallic Ag, and there is no evidence for the presence of Ag$^+$, indicating that the Ag ions in the composites are fully reduced to metallic Ag. Additionally, it is obvious that the peaks of Ag 3d shift to the lower position compared with bulk Ag (368.3 eV for Ag 3d$_{5/2}$, and 374.3 eV for Ag 3d$_{3/2}$), suggesting that the electrons may migrate from the TiO$_2$ particles to metallic Ag,[31] which reveals that there is a strong interaction between Ag nanoparticles and TiO$_2$ particles in the interface of heterostructures.
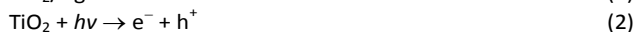
In brief, it can be demonstrated that Ag nanoparticles are grown on the TiO$_2$−treated wood matrix, and there is a strong interaction between Ag and TiO$_2$ in the interface of the Ag−doped TiO$_2$/wood heterostructures. Furthermore, Ag nanoparticles can act as electron acceptors and be advantageous for separating the photo−excited electron−hole pairs, the heterostructures can inhibit the recombination of excited electrons and holes and then enhance the photo−catalytic activity of the products.
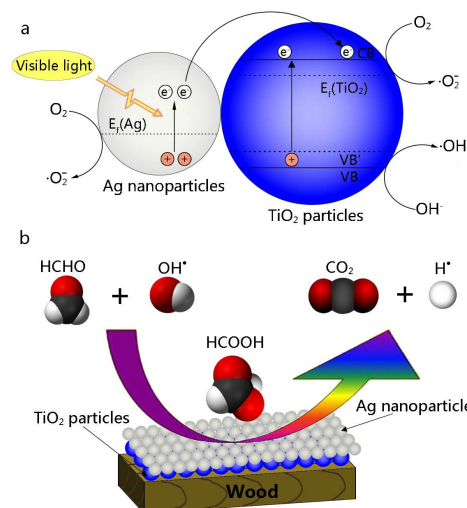
Scheme 3 (a) Proposed photo-induced charge separation and migration process in the Ag−doped TiO$_2$/wood sample under visible−light irradiation, and (b) possible scheme for HCHO adsorption and surface oxidation to CO$_2$ on the surface of Ag−doped TiO$_2$/wood sample.

The probable scheme diagram for the photo−catalytic process of the Ag−doped TiO$_2$/wood sample and a simplified reaction scheme for the catalytic oxidation of HCHO on the surface of the Ag−doped TiO$_2$/wood sample are illustrated in Scheme 3. As shown in Scheme. 3a, during visible−light irradiation, the Ag nanoparticles are photo−excited owing to the plasmon resonance, which the photo−excited electrons are subsequently migrated from the surface of the Ag nanoparticles to the conduction band (CB) of TiO$_2$ particles. In addition, due to the high crystallinity of the Ag nanoparticles, the resistance of the electron migration is decreased leading to a reduction in the recombination of excited electrons and holes. The electrons on the conduction band (CB) of TiO$_2$ are scavenged by dissolved oxygen molecules (O$_2$) and the holes on the valence band (VB) of TiO$_2$ absorb water molecules (H$_2$O) or hydroxyl ions (OH$^−$), which yields abundant of highly oxidative species including superoxide radical anion (·O$_2^−$) and hydroxyl radical (·OH). This causes an improvement of the photo−catalytic performance and aggressive oxidation of the surface−adsorbed toxic organic pollutants (HCHO) to convert into CO$_2$ and water. Furthermore, as revealed by the XPS results, the production of Ti^{3+} species is ascribed to the strong interaction between Ag and TiO$_2$. The energy level of Ti^{3+} species is located between the valence band (VB) and conduction band (CB) of TiO$_2$, which is highly advantageous to promote the electrons in the new valence band (VB') to be excited to the conduction band (CB) of TiO$_2$. Therefore, the Ag nanoparticles can be regarded as electrons trapping centers in the conduction band of TiO$_2$, leading to a decrease in the concentration of photo−induced charge carriers and an enhancement for the photo−catalytic activity of the samples. That is, the migration of charges is enhanced and the recombination of excited electrons and holes is suppressed as a result of the well−known Schottky barrier effect.[14] The

proposed initial elementary reactions are listed in Eqs. (1)–(4) as the followings:

$$TiO_2/Ag + hv \rightarrow e^- + h^+ \tag{1}$$
$$TiO_2 + hv \rightarrow e^- + h^+ \tag{2}$$
$$e^- + O_2 \rightarrow \cdot O_2^- \tag{3}$$
$$h^+ + OH^- \rightarrow \cdot OH + H^+ \tag{4}$$

Moreover, published literatures have described that the mechanism of TiO$_2$ film on decomposition of HCHO.[1, 32, 33] Based on the discussion above, a scheme for HCHO adsorption and surface oxidation to CO$_2$ on the surface of Ag–doped TiO$_2$/wood sample is postulated in Scheme 3b. During the HCHO degradation in the photo–catalytic process, formic acid (HCOOH) is identified as intermediate. The related reactions of HCHO destruction are shown with Eqs. (5)–(9) as the followings:
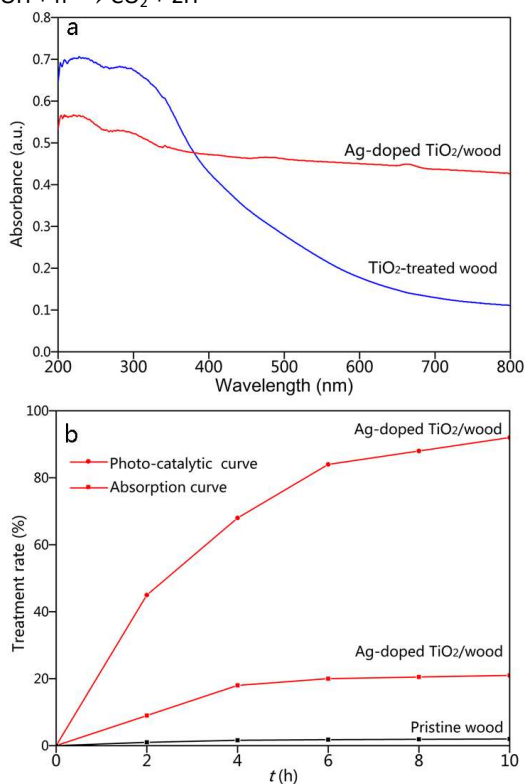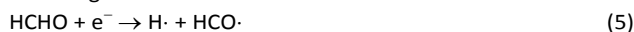
$$HCHO + e^- \rightarrow H\cdot + HCO\cdot \tag{5}$$
$$HCHO + O\cdot \rightarrow OH\cdot + HCO\cdot \tag{6}$$
$$HCHO + OH\cdot \rightarrow HCO\cdot + H_2O \tag{7}$$
$$HCO\cdot + OH\cdot \rightarrow HCOOH \tag{8}$$
$$HCOOH + h^+ \rightarrow CO_2 + 2H\cdot \tag{9}$$

Fig. 5. (a) UV–vis absorption spectra of the TiO$_2$–treated wood and the Ag–doped TiO$_2$/wood, and (b) comparison of adsorption curve and photo–catalytic decomposition curve of HCHO over the pristine wood and the Ag–doped TiO$_2$/wood.

In order to investigate the light absorbance of the samples, the UV–vis diffuse reflection spectra of the TiO$_2$–treated wood and the Ag–doped TiO$_2$/wood are depicted in Fig. 5a. As for the pure TiO$_2$–treated wood, it presents prominent adsorption below 350 nm wavelength. Whereas the Ag–doped TiO$_2$/wood exhibits a much higher absorption in the region 380–800 nm, indicating the absorption of Ag–doped TiO$_2$/wood is significantly red–shifted to the visible due to the

loading of the Ag nanoparticles onto the surface of the TiO$_2$–treated wood. Theoretically, the wide visible absorption should be attributed to the characteristic absorption of surface plasmon resonance originating from the metallic Ag nanoparticles in the Ag–doped TiO$_2$/wood samples. Moreover, it is worth noting that the Ag–doped TiO$_2$/wood heterostructures with absorptions in the visible region may implicate higher activity in photo–catalysis.

Fig. 5b presents comparison of adsorption curve and photo–catalytic degradation curve of HCHO over the pristine wood and the Ag–doped TiO$_2$/wood for every 2 hours. For the pristine wood, both the adsorption and photo–catalytic degradation rate of HCHO is about 2% after 10 h, possibly because the effect of the porous structure of the cell wall of wood is similar to that of active carbon. For the Ag–doped TiO$_2$/wood, in the first two hours, the concentrations of HCHO decreased fast in both cases, and the treatment rate of HCHO by photo–catalytic degradation is still superior to that of HCHO by absorption. Finally, the treatment rate of HCHO by photo–catalytic degradation is 94.9%, while the treatment rate of HCHO by absorption is 21%. The obvious difference between two curves confirms that the photo–catalytic reaction plays an important role in the degradation of HCHO. After 10 h, the absorption curve variation of HCHO is less than 1% and tends to zero. The result indicates the absorption of HCHO over the Ag–doped TiO$_2$/wood reached the adsorption equilibrium. Furthermore, the initial concentrations of the HCHO are 2.14 mg/m^3 for the Ag–doped TiO$_2$/wood in the photo–catalytic degradation reaction. It is obvious that, for the Ag–doped TiO$_2$/wood, the degradation rate of HCHO is dramatically increased, after 6 hours reaction, the degradation rate is slightly decreased but still rising, indicating the photo–catalytic reaction of HCHO is continuing. As well-known, the national regulation illustrates that, for the indoor formaldehyde standard, the HCHO of public places should be below 0.12 mg/m^3, and the HCHO of residential indoors should be below 0.08 mg/m^3. Apparently, the results indicate that the removal efficiency of HCHO by the Ag–doped TiO$_2$/wood under visible–light irradiation could reach the national regulation for the indoor formaldehyde standard of public places, and approximate to the national regulation for indoor formaldehyde standard of residential indoor.

In addition, we further investigated the analogue experiment of formaldehyde degradation by the Ag–doped TiO$_2$/wood under the ultraviolet–germicidal–lamp illumination (365 nm wavelength and approximately 1.5 mW/cm^2 light intensity), as shown in Supplementary Material. Most interestingly, the experimental results present that, for the Ag–doped TiO$_2$/wood, the degradation rate of HCHO driven by UV light is dramatically improved, and the HCHO of 0.72 mg/m^3 in the obturator could be completely eliminated in approximately 1.02 min, elucidating an enhanced photo–catalytic activity of the Ag–doped TiO$_2$/wood under the UV irradiation. Such an important and useful property for the Ag–doped TiO$_2$/wood would greatly promote its application in a fast elimination of HCHO.

RSC Advances

We have also evaluated the reusability of the Ag–doped TiO_2/wood for photo–catalytic degradation of HCHO, as shown in Fig.6. After five cycled runs of the photo–catalytic degradation of HCHO, the photo–catalytic activity of the Ag–doped TiO_2/wood shows great decreases with the degradation rate decreased from 94.9% to 2.2%. It clearly demonstrates that the samples are unstable, because the stability of the wood substrate is not optimistic as the results of the damage of light, moisture, dirt, bacterium, etc.. Hence, further modification with the low–surface–energy materials is necessary to lead to a new durable photo–catalytic material with multifunction, such as superhydrophobicity, superoleophobicity and antibacterial performance. That is, the present study will be a basis of future photo–catalyst development.
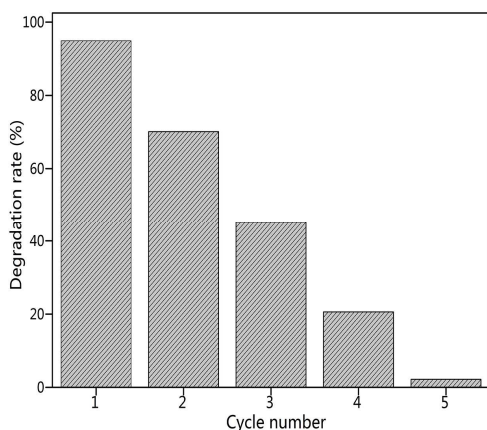

Fig.6. Five cycles of photo–catalytic degradation of HCHO over the Ag–doped TiO_2/wood.

Conclusions

The Heterostructured Ag–doped TiO_2/wood was prepared by a two-step method including the hydrothermal synthesis of TiO_2 particles on the wood substrate and silver mirror reaction of the Ag nanoparticles dopant on the surface of TiO_2/wood. The TiO_2–treated wood and the Ag–doped TiO_2/wood were used in an obturator for HCHO decomposition under visible light. The results indicate that the Ag–doped TiO_2/wood exhibits an enhanced photo–catalytic activity in the decomposition of HCHO driven by the visible light, which is mainly ascribed to the strong interaction between TiO_2 and Ag, and the surface plasmon resonances of Ag nanoparticles excited by visible–light irradiation. Meanwhile, the presence of Ti^{3+} in the Ag–doped TiO_2/wood is advantageous to higher photo–catalytic activity, which extends the photo–response of the products to the visible light. Since the Ag–doped TiO_2/wood enhanced the photo-catalytic degradation of formaldehyde, it would greatly promote the application of the modified wood in a fast elimination of HCHO. However, the stability of the photo–catalyst based on wood substrate requires more exploration in the future researches.

Notes and references

1. W. Liang, J. Li and Y. Jin, *Build. Environ.,* 2012, **51**, 345.
2. O. J. Prado, M. C. Veiga and C. Kennes, *Appl. Microbiol. Biot.,* 2004, **65**, 235.
3. R. B. F. Bulian, S. Ciroi, *Holz. Roh. Werkst.*, 2003, **61**, 3.
4. Z. Wen, L. Tian-mo and L. De-jun, *Physica B,* 2010, **405**, 4235.
5. Y. Liao, C. Xie, Y. Liu, H. Chen, H. Li and J. Wu, *Ceram. Int.,* 2012, **38**, 4437.
6. Q. Yuan, Z. Wu, Y. Jin, L. Xu, F. Xiong, Y. Ma and W. Huang, *J. Am. Chem. Soc.,* 2013, **135**, 5212.
7. S. Wang, H. Qian, Y. Hu, W. Dai, Y. Zhong, J. Chen and X. Hu, *Dalton T.,* 2013, **42**, 1122.
8. J. W. Zhichao Shan, Fangfang Xu, Fu-Qiang Huang, Hanming Ding, *J. Phys. Chem. C*, 2008, **112**, 15423.
9. A. Fujishima, Tata N. Rao, Donald A. Tryk, *J. Photoch. Photobio. C,* 2000, **1**, 1.
10. F. Niu, L. S. Zhang, C. Q. Chen, W. Li, L. Li, W. G. Song and L. Jiang, *Nanoscale*, 2010, **2**, 1480.
11. L. Gao, X. Zhan, Y. Lu, J. Li and Q. Sun, *Mater. Lett.,* 2015, **142**, 217.
12. L. Gao, Y. Lu, X. Zhan, J. Li and Q. Sun, *Surf. Coat. Tech.,* 2015, **262**, 33.
13. Y. Xie and Y. Meng, *RSC Adv.,* 2014, **4**, 41734.
14. C. Su, L. Liu, M. Zhang, Y. Zhang and C. Shao, *CrystEngComm*, 2012, **14**, 3989.
15. S. Z. Chu, K. Wada, S. Inoue, S. I. Hishita and K. Kurashima, *J. Phys. Chem. B*, 2003, **107**, 10180-10184.
16. P. Zhang, J. Guo, P. Zhao, B. Zhu, W. Huang, and S. Zhang, *RSC Adv.*, 2015.
17. G. Sahu, Scott W. Gordon and Matthew A. Tarr. *RSC Adv.*, 2012, **2**, 573.
18. Y. Bessekhouad, D. Robert and J. V. Weber. *J. Photoch. Photobio. A*, 2004, **163**, 569-580.
19. X.Lin, J. Xing, W. Wang, Z. Shan, F. Xu and F. Huang, *J. Phys. Chem. C*, 2007, **111**, 18288-18293.
20. J. Yu, L. Qi and M. Jaroniec, *J. Phys. Chem. C*, 2010, **114**, 13118.
21. S. Chen, Y. Li and C. Wang, *RSC Adv.*, 2015, **5**, 15880.
22. Q. Zhang, J. Ye, P. Tian, X. Lu, Y. Lin, Q. Zhao and G. Ning, *RSC Adv.*, 2013, **3**, 9739.
23. P. Davide Cozzoli, E. Fanizza, R. Comparelli, M. Lucia Curri and A. Agostiano, *J. Phys. Chem. B*, 2004, **108**, 9623.
24. M. K. Seery, R. George, P. Floris and S. C. Pillai, *J. Photoch. Photobio. A*, 2007, **189**, 258.
25. C. Jin, C. Li, S. Han, J. Wang, Q. Yao and Q. Sun, *J. Alloy. Compd.* 2015, **635**, 300.
26. T. Yuan, B. Zhao, R. Cai, Y. Zhou and Z. Shao, *J. Mater. Chem.,* 2011, **21**, 15041.
27. S. Andersson, R. Serimaa, T. Paakkari, P. SaranpÄÄ and E. Pesonen, *J. Wood Sci.,* 2003, **49**, 531.
28. B. K. Sarma, A. R. Pal, H. Bailung and J. Chutia, *J. Phys. D: Appl. Phys.,* 2012, **45**, 275401.
29. L. Zhang, L. Chen, L. Chen and G. Zhu, *RSC Adv.,* 2014, **4**, 54463.
30. K. Siuzdak, M. Sawczak, M. Klein, G. Nowaczyk, S. Jurga

and A. Cenian, *Phys. Chem. Chem. Phys.,* 2014, **16**, 15199.

31.   C. Wang, Y. E, L. Fan, S. Yang and Y. Li, *J. Mater. Chem.,* 2009, **19**, 3841.

32.   Y. Sekine, *Atmos. Environ.,* 2002, **36**, 5543.

33.   Ching-Feng Mao and M. Albert Vannice, *J. Catal.,* 1995, **154**, 230.